Published in final edited form as:
Nat Neurosci. 2004 October ; 7(10): 1079–1087.

Essential role of Ca^{2+}-binding protein 4, a $Ca_v1.4$ channel regulator, in photoreceptor synaptic function

Françoise Haeseleer[1,6], **Yoshikazu Imanishi**[1,6], **Tadao Maeda**[1], **Daniel E Possin**[1], **Akiko Maeda**[1], **Amy Lee**[2], **Fred Rieke**[3], and **Krzysztof Palczewski**[1,4,5]

[1]*Department of Ophthalmology, University of Washington, Box 356485, Seattle, Washington 98195, USA.* [2]*Department of Pharmacology and Center for Neurodegenerative Disease, Emory University School of Medicine, Atlanta, Georgia 30322, USA.* [3]*Departments of Physiology and Biophysics,* [4]*Pharmacology and* [5]*Chemistry, University of Washington, Seattle, Washington 98195, USA.*

Abstract

CaBP1–8 are neuronal Ca^{2+}-binding proteins with similarity to calmodulin (CaM). Here we show that CaBP4 is specifically expressed in photoreceptors, where it is localized to synaptic terminals. The outer plexiform layer, which contains the photoreceptor synapses with secondary neurons, was thinner in the *Cabp4*$^{-/-}$ mice than in control mice. *Cabp4*$^{-/-}$ retinas also had ectopic synapses originating from rod bipolar and horizontal cells that extended into the outer nuclear layer. Responses of *Cabp4*$^{-/-}$ rod bipolars were reduced in sensitivity about 100-fold. Electroretinograms (ERGs) indicated a reduction in cone and rod synaptic function. The phenotype of *Cabp4*$^{-/-}$ mice shares similarities with that of incomplete congenital stationary night blindness (CSNB2) patients. CaBP4 directly associated with the C-terminal domain of the $Ca_v1.4$ α_1-subunit and shifted the activation of $Ca_v1.4$ to hyperpolarized voltages in transfected cells. These observations indicate that CaBP4 is important for normal synaptic function, probably through regulation of Ca^{2+} influx and neurotransmitter release in photoreceptor synaptic terminals.

L-type Ca^{2+} channels are involved in neuronal differentiation and outgrowth and in synaptic plasticity[1,2]. At many ribbon synapses, Ca^{2+} influx through L-type Ca^{2+} channels triggers neurotransmitter release[3–5]. The α_1-subunit of the L-type $Ca_v1.4$ channel ($Ca_v1.4\alpha1$) is specific to photoreceptors and is present at highest density in the synaptic terminals[5,6]. Compared with other L-type Ca^{2+} channels, $Ca_v1.4$ channels are activated at relatively more negative voltages and show slow inactivation[7–9], important properties for the ability of photoreceptors to sustain continual glutamate release in the dark[4,10]. Null mutations in $Ca_v1.4\alpha1$ are responsible for an X-linked disorder, CSNB2 (refs. 11,12). ERGs of these patients indicate that a deficit may occur in transmission of signals from rod photoreceptors to bipolar cells. In mice, deletion of the β_2-subunit, another component of the photoreceptor L-type channel, alters the expression of $Ca_v1.4$ and produces a phenotype similar to that seen in CSNB2 patients[13].

CaBPs, a subfamily of calmodulin (CaM)-like neuronal Ca^{2+}-binding proteins[14], modulate voltage-dependent Ca^{2+} channels (VDCCs) and inositol triphosphate receptors[15–17]. Here we show that CaBP4, which has only been partially characterized *in silico*[14], is found specifically

Correspondence should be addressed to F.H. (fanfan@u.washington.edu) and K.P. (palczews@u.washington.edu)..
[6]These authors contributed equally to this work.

Note: Supplementary information is available on the Nature Neuroscience website.

COMPETING INTERESTS STATEMENT
The authors declare that they have no competing financial interests.

in photoreceptor synaptic terminals, is important for the normal function of photoreceptor synapses and colocalizes with and modulates the activity of expressed $Ca_v1.4$ channels. These results indicate that CaBP4 may be an important regulator of Ca^{2+} influx and transmitter release in photoreceptor synaptic terminals.

RESULTS

CaBP4 is a CaM-related CaBP

CaBP4 was identified by polymerase chain reaction (PCR) cloning using primers based on the sequence of its closest relative, CaBP2 (ref. 14). The full-length cDNA of human CaBP4 contains an open reading frame of 825 bp, predicting a protein of 275 amino acids and a calculated molecular mass of 30,432 Da. Human, bovine, mouse and rat CaBP4 are highly homologous in their C-terminal regions (~90%) and are less conserved in their N-terminal regions (~60%) with inter-species differences occurring in the first exon (Fig. 1a). CaBP4 contains four EF-hand motifs, although the second motif cannot coordinate Ca^{2+} because the Lys residue in position 1 is not suitable for Ca^{2+} coordination (Fig. 1a).

The *Cabp4* gene is short (~4 kb) with a six-exon structure similar to CaM (see **Supplementary Fig. 1** online). The human genome data at the NCBI predict that *Cabp4* is in the opposite orientation and is separated by four genes and ~60 kb from *Cabp2* on chromosome 11 at q13.1, a region with conserved synteny with mouse chromosome 19.

CaBP4 is localized in rod and cone photoreceptor synapses

Northern blot analyses with the CaBP4 cDNA probe showed two transcripts of 1.6 kb and 3.8 kb in the retina (Fig. 1b). CaBP4 products from PCR with reverse transcription (RT-PCR) were observed in the retina but not in other locations (Fig. 1c). The CaBP4 antisense RNA probe hybridized to the mouse photoreceptor inner segments (Fig. 1d). CaBP4 was expressed in monkey rods and cones; *in situ* hybridization coupled with immunocytochemistry confirmed the expression of monkey CaBP4 in all cone types (Fig. 1e). CaBP4 was not detected in retinal cells other than photoreceptors (Fig. 1d,e).

Subcellular localization of CaBP4 in the mouse retina was carried out using specific antibodies to CaBP4. The staining pattern with these antibodies was compared with the localization of PSD95 (Fig. 1f), a presynaptic protein that is found in terminals from both types of photoreceptor[18]. CaBP4 was observed in both rod spherules and cone pedicles (Fig. 1f). The presynaptic localization of CaBP4 was confirmed using double-labeling studies with antibodies to synaptic vesicle protein SV2 and synaptophysin (Fig. 1g).

Cabp4$^{-/-}$ mice have abnormal outer plexiform layers

CaBP4-deficient mice were generated by replacing exon 1 and part of exon 2 with the PGK-*neo* cassette (**Supplementary Fig. 1**). A PCR-based assay confirmed the disruption of *Cabp4* in *Cabp4*$^{-/-}$ mice (**Supplementary Fig. 1**). CaBP4 proteins were not detected in *Cabp4*$^{-/-}$ retinas by immunoblotting or immunocytochemistry (Fig. 2a,b).

Retinal morphologies of 2-month-old *Cabp4*$^{-/-}$ and *Cabp4*$^{+/+}$ mice were compared using light and electron microscopy. Structural changes were observed in the outer segment and outer nuclear layers: rod outer segments were shorter, the disk density was lower and the outer nuclear layer was missing one or two layers of cell bodies. The outer segments of *Cabp4*$^{-/-}$ mice were 15% shorter than those of *Cabp4*$^{+/+}$ mice (Fig. 2d; averages of rod outer-segment thickness at 250–2,000 μm from the optic nerve were compared). This observation is consistent with a similar drop in rhodopsin content as measured directly by UV-visible spectroscopy and retinoid analysis (data not shown)[19].

Marked changes were observed in the outer plexiform layer, which showed ~51% reduction in thickness in *Cabp4*$^{-/-}$ mice as compared with *Cabp4*$^{+/+}$ mice ($P < 0.001$; Fig. 2e; averages of outer-plexiform-layer thickness at 250–2,000 μm from the optic nerve were compared). Quantitative calculations of the thickness of other retinal layers showed no significant differences between these two genetic backgrounds ($P > 0.05$; Fig. 2c). Electron micrographs showed a paucity of photoreceptor terminals and synaptic ribbons in the outer plexiform layer of *Cabp4*$^{-/-}$ mice (Fig. 2f,g and **Supplementary Fig. 2**). Quantitative analysis of the electron micrographs showed that the number of photoreceptor terminals was ~33% lower in *Cabp4*$^{-/-}$mice (251 ± 59 photoreceptor terminals, $n = 3$ mice) as compared with *Cabp4*$^{+/+}$ mice (372 ± 17, $n = 3$ mice), and the number of synaptic ribbons was 37 ± 14% ($n = 3$ mice) lower in *Cabp4*$^{-/-}$ mice. These data indicate that the photoreceptor terminals are both less numerous and defective. Changes in the outer plexiform layer were more pronounced in 6- to 8-month-old *Cabp4*$^{-/-}$ mice than in 2-month-old mice (**Supplementary Figs. 2 and 3**).

To investigate the consequence of CaBP4 deficiency on synapses of the outer plexiform layer in more detail, we analyzed synaptic morphology in *Cabp4*$^{-/-}$ mice using antibodies that label specific synaptic proteins or cell types. In *Cabp4*$^{+/+}$ and *Cabp4*$^{-/-}$ mice, the ionotropic glutamate receptor 1 was highly concentrated at postsynaptic sites(Fig. 3a). Photoreceptor synaptic terminals were visualized using antibody to PSD95 (anti-PSD95; ref. [18]; Fig. 3a,**b**). In *Cabp4*$^{+/+}$ mice, rod spherules and cone pedicles were inflated, whereas those in *Cabp4*$^{-/-}$ mice were disorganized and flat (also see **Supplementary Fig. 3**). mGluR6 immunoreactivity[21] was aggregated in hot spots at the tips of dendritic processes in both *Cabp4*$^{+/+}$ and *Cabp4*$^{-/-}$ mice (Fig. 3b). Fewer hot spots were observed, however, in *Cabp4*$^{-/-}$ mice. mGluR6 localized proximally to PSD95 (Fig. 3b) in both cases.

An antibody to bassoon (anti-bassoon), which is a presynaptic cytomatrix protein[22], labeled horseshoe-shaped structures in *Cabp4*$^{+/+}$ mice but produced only punctuate staining in *Cabp4*$^{-/-}$mice (Fig. 3c). In addition, some labeled puncta in *Cabp4*$^{-/-}$ retinas were located in the outer nuclear layer. The number of bassoon-positive presynaptic terminals in the outer plexiform layer and outer nuclear layer were compared between *Cabp4*$^{-/-}$ and *Cabp4*$^{+/+}$ mice. A decrease of 43.7 ± 13.7% (mean ± s.d.; $n = 3$) in the number of presynaptic terminals was observed (in a cross-section of the retina, ~1,250 μm from the optic nerve head).

Dendrites of rod bipolar cells that were visualized using an antibody to PKCα were poorly branched and underdeveloped in *Cabp4*$^{-/-}$ mice as compared with *Cabp4*$^{+/+}$ mice (Fig. 3e,**f**). In some instances, bipolar and horizontal cell dendrites extended into the outer nuclear layer of *Cabp4*$^{-/-}$ mice and formed ectopic synapses with photoreceptors (Fig. 3d,f); such branching was never observed in *Cabp4*$^{+/+}$ mice, in which dendritic processes of rod bipolar and horizontal cells ended at the outer plexiform layer (Fig. 3d,e).

Visual responses in *Cabp4*$^{-/-}$ mice are abnormal

The disruption of normal synaptic morphology in *Cabp4*$^{-/-}$ mice indicates that corresponding deficits in synaptic function may be present. Indeed, as described below, transmission from rods and cones to bipolar cells was severely attenuated in *Cabp4*$^{-/-}$ mice, whereas photoreceptor responses were only modestly affected.

We compared responses of rod photoreceptors from *Cabp4*$^{+/+}$ and *Cabp4*$^{-/-}$ mice using suction electrode recordings[23]. At all flash strengths, the responses of *Cabp4*$^{-/-}$ rods were faster and less sensitive than the corresponding *Cabp4*$^{+/+}$ responses (Fig. 4a,b). The difference in sensitivity was quantified by fitting each cell's stimulus-response relationship to determine the flash that produced a half-maximal response (Fig. 4c). The half-saturating flash strength was 9.4 ± 0.5 Rh* for *Cabp4*$^{+/+}$ rods (mean ± s.e.m.; $n = 22$) and 13.4 ± 0.6 Rh* for *Cabp4*$^{-/-}$ rods ($n = 38$). The difference in kinetics was characterized by measuring the time to peak and

integration time of responses to dim flashes. *Cabp4*$^{-/-}$ rods had a shorter time to peak (171 ± 5 ms in 31 *Cabp4*$^{-/-}$ rods versus 220 ± 11 ms in 25 *Cabp4*$^{+/+}$ rods; mean ± s.e.m.) and smaller integration time (210 ± 17 ms versus 340 ± 22 ms). We do not know what causes the difference between light responses in *Cabp4*$^{-/-}$ and *Cabp4*$^{+/+}$ rods; changes in outer-segment Ca^{2+} dynamics, as measured from exchange currents[24], were not significantly different (data not shown).

To determine whether signal transfer from rods to rod bipolar cells was altered in *Cabp4*$^{-/-}$ mice, we measured light responses of rod bipolar cells in a retinal slice preparation[25]. *Cabp4*$^{+/+}$ rod bipolars had maximal responses of up to 400 pA (n = 47), whereas *Cabp4*$^{-/-}$ rod bipolars had maximal responses of at most 12 pA (n = 52; Fig. 5a,b). Furthermore, the half-saturating flash strength was higher for *Cabp4*$^{-/-}$ rod bipolars than for *Cabp4*$^{+/+}$ cells (Fig. 5d). The half-saturating flash strength was 2.8 ± 0.04 Rh*/rod (mean ± s.e.m.; n = 30) in *Cabp4*$^{+/+}$ rod bipolars and 25 ± 3 Rh*/rod in *Cabp4*$^{-/-}$ rod bipolars (n = 16). The increased half-saturating flash strength and decreased maximal response cause the sensitivity of *Cabp4*$^{-/-}$ rod bipolars to be at least 100-fold less than that of *Cabp4*$^{+/+}$ cells (Fig. 5c). Because the rod responses in the two mouse strains differed by a factor of close to two, this large difference in the rod bipolar responses indicates a deficit in synaptic transmission.

Rod bipolar cells use mGluR6 metabotropic glutamate receptors to detect glutamate released from the rods[21]. Activation of these receptors leads to closure of nonselective cation channels. To determine what fraction of these channels was closed in darkness, we exposed rod bipolars to a saturating concentration of the mGluR6 agonist APB[26], which creates a high level of activity in the transduction cascade that links receptors and channels and closes most or all of the open channels[27].

As expected, APB eliminated the light response in a *Cabp4*$^{+/+}$ rod bipolar cells by activating mGluR6 receptors and rendering them insensitive to changes in glutamate (Fig. 5e). APB also produced a minimal change in dark current, as previously reported[27]. APB again eliminated the light response in a *Cabp4*$^{-/-}$ rod bipolar cell but also produced a large decrease in the inward dark current (Fig. 5f). In *Cabp4*$^{+/+}$ rod bipolar cells, the change in saturating response was more than 50 times the change in dark current[27]. In *Cabp4*$^{-/-}$ rod bipolar cells, the change in dark current produced by APB was similar in magnitude to the saturating light response (n = 18). Thus, the number of additional channels open at the peak of the saturating light response was comparable to the number that were open in darkness in *Cabp4*$^{-/-}$ rod bipolars. This indicates that the glutamate concentration present at the mGluR6 receptors is substantially lower in *Cabp4*$^{-/-}$ rod bipolars as compared with that in *Cabp4*$^{+/+}$ cells.

Disruption of cone and rod signaling

ERG responses in *Cabp4*$^{-/-}$ mice and *Cabp4*$^{+/+}$ mice confirmed the differences described above for rod signaling and indicated a similar disruption of signaling between cones and cone bipolar cells. The a-wave (generated by photoreceptors) of dark-adapted *Cabp4*$^{-/-}$ mice was about half the amplitude of that of *Cabp4*$^{+/+}$ mice (Fig. 6a,b and **Supplementary Fig. 4**). The b-wave (the bipolar cell component) was dramatically reduced in *Cabp4*$^{-/-}$ mice. In some cases, a small positive voltage change remained in the normal location of the b-wave, indicating that some transmission remained between photoreceptor and bipolar cells.

Under light-adapted conditions, the a-waves of *Cabp4*$^{-/-}$ and *Cabp4*$^{+/+}$ mice differed by ~20%, suggesting that cone function was near normal (Fig. 6c,d). The b-wave was significantly reduced at all stimulus intensities in *Cabp4*$^{-/-}$ mice as compared with *Cabp4*$^{+/+}$ mice. Thus, the absence of CaBP4 disrupted normal transmission of signals from rods and cones to bipolar cells.

CaBP4 interacts with and modulates $Ca_v1.4$

L-type VDCCs are modulated by CaM, which binds to multiple sites in the C-terminal domain of the α_1-subunit[28–30]. CaBP1 interacts with and modulates $Ca_v2.1$ channels[15] and $Ca_v1.2$ channels[31]. To test whether CaBP4 might have a similar role, we monitored direct interactions between CaBP4 and a cytoplasmic fragment of $Ca_v1.4\alpha1$. We coupled the $Ca_v1.4\alpha1$ fragment (amino acids 1445–1983) to a resin and loaded purified CaBP4 in the presence of Ca^{2+}. CaBP4 bound to the $Ca_v1.4\alpha1$ C terminus in a Ca^{2+}-dependent manner as shown by EGTA elution, but a significant fraction of the protein bound to the column in a Ca^{2+}-independent manner as shown by subsequent acid elution (Fig. 7a).

To further investigate if CaBP4 interacts with $Ca_v1.4$ in a more physiological setting, we analyzed the colocalization of these proteins in transfected HEK293 cells. To visualize the proteins, we constructed enhanced green fluorescent protein (EGFP) and DsRed2 fusion proteins. When HEK293 cells were transfected with mCaBP4-DsRed2, the red fluorescence was detected throughout the cytoplasm (Fig. 7b). Expression of $Ca_v1.4$-GFP with mCaBP4-DsRed2 resulted in localization of mCaBP4-DsRed2 with $Ca_v1.4$-GFP to the plasma membrane (Fig. 7b), indicating that these two proteins may interact with each other in HEK293 cells.

To test whether CaBP4 altered the function of $Ca_v1.4$ channels, we analyzed whole-cell patch-clamp recordings of Ca^{2+} currents in transfected HEK293T cells. In cells transfected with $Ca_v1.4$ alone, inward Ca^{2+} currents were evoked from a holding voltage of −80 mV to a range of voltages from −30 to +60 mV (Fig. 7c,d). $Ca_v1.4$ showed virtually no inactivation during 50-ms step depolarizations, as described previously[7–9]. In cotransfected cells, CaBP4 enhanced activation of $Ca_v1.4$ by shifting the *I-V* relationship to hyperpolarized voltages (Fig. 7c,d). Maximal inward current was evoked at significantly more negative voltages in cells cotransfected with CaBP4 ($V_{half} = -15.4 \pm 1.2$, $V_{max} = 7.8 \pm 1.6$ mV, $n = 7$) as compared with cells transfected with $Ca_v1.4$ alone ($V_{half} = -5.3 \pm 1.9$, $V_{max} = 17.2 \pm 1.3$ mV, $n = 10$; $P < 0.05$).

DISCUSSION

CaBP4 is a photoreceptor-specific protein that belongs to a subfamily of at least eight CaM-related proteins[14–17]. The specific functions of these proteins *in vivo* remain unclear, although *in vitro* CaBP1 interacts with inositol triphosphate receptors and $Ca_v2.1$ channels[15–17] and with $Ca_v1.2$ channels[31]. The work presented here shows that CaBP4 is essential for the development and/or maintenance of the photoreceptor output synapse, probably through modulation of photoreceptor Ca^{2+} channels and transmitter release.

CaBP4 is important for synapse formation and function

Photoreceptor synapses in CaBP4-deficient mice were severely disrupted both anatomically and functionally. *In situ* hybridization and confocal microscopy showed that CaBP4 was located specifically in photoreceptors, and primarily in their synaptic terminals. Light and electron microscopy showed dramatic changes in photoreceptor synapses, including a thinner outer plexiform layer, a reduction in the number of synaptic ribbons and photoreceptor terminals and deflation of rod spherules and cone pedicles. The absence of CaBP4 also resulted in the formation of ectopic synapses between rods and rod bipolar or horizontal cells in the outer nuclear layer. Ectopic synapses are also present in mice that are deficient in the bassoon protein, which is required for the anchoring of the photoreceptor ribbon to the active zone[22]. Although the morphology of the retina and outer plexiform layer are preserved in Bassoon-deficient mice, ERG recordings show that the transfer of signals from photoreceptors to postsynaptic cells is attenuated[22].

Light responses of CaBP4-deficient mice were also altered as compared with those of control mice. Single-cell recordings and ERG measurements showed a disruption in the transmission of photoreceptor signals to postsynaptic cells. In darkness, a significant fraction of the cation channels that were coupled to mGluR6 receptors were open in rod bipolar cells of CaBP4-deficient mice, unlike those in control rod bipolars[27]. Thus, the glutamate concentration that was present at the bipolar mGluR6 receptors was reduced in the absence of CaBP4.

CaBP4 modulates Cav1.4

CaBP4 colocalized and interacted with expressed $Ca_v1.4$ VDCCs and modulated their functional properties. Thus, like CaM[15], CaBPs may be physiological regulators of VDCCs.

The photoreceptor Ca^{2+} currents activate at voltages of 10–15 mV more negative than currents obtained after heterologous expression of $Ca_v1.4$ (ref. 8). The voltage dependence of heterologously expressed $Ca_v1.4$ channels would be poorly suited to control transmitter release at physiological voltages for photoreceptors. The absence of a cytosolic modulator might explain the difference between native and recombinant channels. Indeed, CaBP4 shifted the activation range of expressed L-type VDCCs to more hyperpolarized voltages, suggesting that CaBP4 is a modulator of Cav1.4 *in vivo*. As a consequence of this voltage shift, at the photoreceptor resting potential of approximately −40 mV[32], Ca^{2+} influx through expressed L-type VDCCs increased about fivefold in the presence of CaBP4 as compared with its absence. This change in Ca^{2+} influx should produce a corresponding change in transmitter release, which is consistent with the lowered activity of mGluR6 receptors observed in *Cabp4*$^{-/-}$ rod bipolar cells.

The IQ motifs and the regions known to bind CaM and to be necessary for Ca^{2+}-dependent inactivation[28–30,33,34] are conserved between the α_1-subunits of the L-type VDCCs, suggesting that $Ca_v1.4$ might also be modulated by CaM or by a CaM-like protein. Apo-CaM is tethered to L-type VDCCs in its resting state. The tethering is to two peptides located upstream from the IQ motif in the cytoplasmic C-terminal part of the channel α_1-subunit28. CaBP4 also bound to $Ca_v1.4$ in the absence of Ca^{2+}, although less effectively than in the presence of Ca^{2+} (Fig. 7a). It is possible that CaBP4 is also tethered to the channel in its resting state.

Interaction of CaBP4 with L-type VDCCs could lead to a variety of effects that are necessary for proper formation of the photoreceptor synapse. L-type VDCCs are essential in the development of neuritic outgrowth in several neuronal cell types[2]. In rods, L-type VDCCs are the primary Ca^{2+} channels required for structural plasticity and upregulation of synaptic vesicle synthesis[1,2]. A splice variant of CaBP1, caldendrin, colocalizes with synaptophysin in the inner plexiform layer and might be involved in the development of amacrine cell processes before functional synapses have formed[35]. L-type VDCCs also activate signaling pathways that lead to transcriptional activation[36]. The cAMP response element–binding proteins, which drive the expression of a number of genes that regulate neuronal survival and plasticity[37,38], and MEF-2, a MADS transcription factor that mediates neuronal survival[39], depend on Ca^{2+} flux through L-type VDCCs.

Although the molecular identity of the cone Ca^{2+} channels is not fully elucidated, some cone channels contain the $Ca_v1.3$ subunit[5,40,41]. The disruption of cone signaling in CaBP4-deficient mice indicates that CaBP4 is also critical for the normal development of cone synaptic terminals. The peptide sequences of $Ca_v1.4$ that bind CaM are conserved in the $Ca_v1.4$ and the $Ca_v1.3$ α1-subunits. $Ca_v1.4$ is also expressed in retinal bipolar cells[42]. CaBP1, 2 and 5, which are members of the same neuronal CaBP subfamily as CaBP4, are expressed in other neurons including the cone and rod bipolar cells[14]. A similar mode of regulation of calcium channels by CaBPs might also occur in other neurons.

The phenotype of *Cabp4*$^{-/-}$ mice resembles that observed in CSNB2 patients carrying mutations in the gene *CACNA1F*[12,43] and in mice deficient for the β_2-subunit of the $Ca_v1.4$ channel[13]. CSNB2 patients show reduced b-wave and impaired rod and cone function. The β_2-subunit-deficient mice show downregulation of $Ca_v1.4$ α1-subunit and have a normal a-wave, a highly reduced b-wave and a thinner outer plexiform layer. Both of these channel disruptions may lead to a reduction in Ca^{2+} influx and transmitter release from photoreceptor synaptic terminals, which in turn disrupts normal synaptic development and function.

METHODS

Cloning of CaBP4 and $Ca_v1.4$ α1-subunit.

A partial cDNA clone encoding CaBP4 was amplified from a human retina cDNA library using primers based on CaBP2. The full-length cDNA sequence was isolated as two overlapping fragments by nested PCR from retinal cDNA libraries using primers that hybridized to the arm of the vector and CaBP4 sequence. The PCR products were cloned in *pCRII-TOPO* vector (Invitrogen) and were sequenced using the DyeDeoxyTerminator method (ABI-Prism, Perkin Elmer).

After removal of the stop codon by PCR, the mouse CaBP4 was cloned with a fragment encoding a $(Gly)_7$-Leu-$(Gly)_7$ fused to Ds-Red in pFastCMV44. Recombinant baculovirus carrying this fusion protein under the control of the CMV promoter was prepared as described previously[44].

The mouse $Ca_v1.4α1$ gene was cloned in four fragments from mouse retina RNA by RT-PCR using primers based on published sequences; it encodes a protein of 1,984 amino acids that are identical to sequence for AJ579852 (ref. 8). The full-length coding sequence was put together into *pcDNA3.1(−)*. For fusion to EGFP, mouse $Ca_v1.4α1$ was cloned in *pEGFP-C2* (Clontech). The β_{2A}- and $\alpha_2\delta$-subunits were cloned into *pcDNA3.1(+)*[45,46].

Tissue distribution of CaBP4.

Rat retina and brain mRNAs, and tissue northern blot containing 2 μg of poly(A)$^+$ RNA from various human tissues were purchased from Clontech Laboratories. Northern blots were probed with ^{32}P-labeled *CABP4*, *Cabp4* or *ACTB* DNAs (encoding human and mouse CaBP4 and human β-actin, respectively)[47]. In addition, the tissue distribution was analyzed by RT-PCR with primers designed to amplify the complete mouse CaBP4 coding sequence as described previously[14].

Expression of CaBP4 and the C-terminal fragment of $Ca_v1.4α1$ in bacteria.

His-tagged CaBP4 and $Ca_v1.4α1$ partial peptides were generated by cloning appropriate PCR fragments into *pET30b* (Novagen). The proteins were expressed in BL21 bacteria after induction with 0.2 mM IPTG and were purified on Ni^{2+}-NTA columns according to the manufacturer's protocol (Qiagen).

Transfection of $Ca_v1.4$-EGFP and CaBP4-DsRed2 in HEK293 cells.

HEK293 cells were transfected with $Ca_v1.4$-EGFP using Geneporter 2 reagent (Gene Therapy Systems) according to the manufacturer's instructions. At 24 h after transfection, the cells were incubated with *pFastCMV-mCaBP4-DsRed2* baculovirus for 5 h. The cells were incubated for an additional 2 d before fixation in 4% paraformaldehyde and analysis on a Zeiss LSM510 laser-scanning microscope (Carl Zeiss).

Antibody production.

Rabbit polyclonal antibodies against bacterially expressed full-length mouse CaBP4 (sera UW145 and UW146) were raised in New Zealand white rabbits as described previously[14]. Monoclonal mouse anti-PSD95 (clone K28/43) was purchased from Upstate Biotechnology. Monoclonal mouse anti–protein kinase C (clone MC5) was purchased from Sigma. Anti-synaptophysin was purchased from Sigma. Monoclonal mouse anti-bassoon antibody was purchased from Stressgen. Rabbit anti-GluR1 was purchased from Chemicon. Monoclonal mouse anti-calbindin (clone CL-300) was purchased from Sigma Immunochemicals.

CaBP4 knockout mice.

The targeting vector was constructed by replacing exon 1 and part of exon 2 with the *neo* gene cassette (**Supplementary Fig. 1**). The mice were generated as described in the legend to **Supplementary Figure 1b**. The *Cabp4*-targeted allele was maintained in a C57Bl/6J background. All procedures using mice were approved by the University of Washington Institutional Animal Care and Use Committee.

Histology, immunocytochemistry and *in situ* hybridization.

For histology, we fixed eyecups in 2% glutaraldehyde/2% paraformaldehyde for 18 h. For immunocytochemistry and *in situ* hybridization, we fixed eyecups in 4% paraformaldehyde in 0.1 M phosphate buffer (PB) for 8 h. After fixation, tissues were infiltrated with 20% sucrose in PB and then were embedded in 33% OCT compound (Miles) diluted with 20% sucrose in PB. We cut 10-μm sections for immunocytochemistry and *in situ* hybridization.

For histology, we cut sections at 5 μm, stained them with hematoxylin (Harris modified hematoxylin solution; Sigma) and viewed them with Nomarski optics (labophot-2, Nikon). Images were captured with a digital CCD (charge-coupled device) camera (Diagnostic Instruments). Probe synthesis and *in situ* hybridization for retinal sections were as previously described[48].

Immunocytochemistry was carried out as described previously[48]. For double staining, a mixture of Cy3-conjugated goat anti–rabbit IgG and Alexa488–conjugated goat anti–mouse IgG was used. Sections were occasionally stained with Hoechst 33342 dye (Molecular Probes). Sections were analyzed under a confocal microscope (Zeiss LSM510, Carl Zeiss). Three-dimensional reconstructions (Fig. 3) were made using LSM510 software 3.0.

Transmission electron microscopy.

Tissue preparation and electron microscopy were carried out as described previously[49]. Photoreceptor terminals and synaptic ribbons were counted from working prints of sections obtained from three mice and at two different positions (~20 μm apart). Sections of ~800 μm were analyzed from one end to the other.

Affinity chromatographies.

Purified His-tagged mCaBP4 was loaded onto a Cav1.4α1 C terminus (amino acid 1445–1983)-Sepharose column that was equilibrated with 10 mM 1,3-bis[tris(hydroxymethy)methylamino] propane (BTP) (pH 7.5), 2 mM benzamidine and 0.1 mM $CaCl_2$. The column was then washed successively with the same buffer containing 150 mM NaCl. The elution was done with 3 mM EGTA followed by 0.1 M Gly, pH 2.5. Fractions (1 ml) were collected and aliquots were analyzed by SDS-PAGE.

ERGs.

ERGs were recorded from anesthetized mice as described previously[50]. Leading edges of the ERG responses were fitted (as an ensemble) with a model of rod phototransduction activation as previously described[19]. C57Bl/6NCrlBr mice were used as controls.

Recordings from rods and rod bipolar cells.

Suction electrode recordings from rod photoreceptors and patch-clamp recordings from rod bipolar cells followed published procedures[27]. C57Bl/6J mice were used as controls. Rod and rod bipolar responses were each measured from four mice that were dark adapted for at least 12 h. For rod bipolar experiments, three or four slices were examined from each mouse. Photon densities measured at the preparation were converted to photoisomerizations per rod (Rh*/rod) assuming a collecting area of 0.5 μm^2 (ref. 25). All experiments were at 35–37 °C.

Whole-cell patch-clamp recordings.

HEK293T cells were grown to ~70–80% confluence and were transfected with Gene Porter reagent (Gene Therapy Systems) according to manufacturer's protocols. Cells were plated on 35-mm dishes and were transfected with a total of 5 μg DNA ($\alpha_1$1.4, β_{2A}, $\alpha_2\delta$ ± CaBP4) including 0.3 μg of *pEGFP–N1* for fluorescence detection of transfected cells. At least 48 h after transfection, we acquired whole-cell patch-clamp recordings of transfected cells with a HEKA EPC-9 patch-clamp amplifier (HEKA Instruments). Data acquisition and leak subtraction using a P/−4 protocol were done with Pulse software (HEKA Instruments). Extracellular recording solutions contained 140 mM Tris, 2 mM $MgCl_2$ and 20 mM $CaCl_2$. Intracellular solutions consisted of 140 mM *N*-methyl-$_D$-glucamine, 10 mM 4-(2-hydroxyethyl)-1-piperazineethanesulfonic acid, 2 mM $MgCl_2$, 2 mM Mg-ATP and 5 mM EGTA. The pH of recording solutions was adjusted to 7.3 with methanesulfonic acid. *I-V* curves were fitted according to the following relationship: $I = G_{max}(V-V_{rev})/(1+\exp\{(V_{half}-V)/k_{act}\})$, where V_{rev} is the extrapolated reversal potential for I_{Ca}, V is the test voltage, I is the peak current, G_{max} is the maximum conductance, V_{half} is the voltage for half-maximal activation and k_{act} is the slope factor. Data were analyzed using Igor software (Wavemetrics) and graphs and statistical analyses were done with Sigma Plot (SPSS).

Statistical analyses.

A one-way analysis of variance was used for statistical analyses.

Supplementary Material

Refer to Web version on PubMed Central for supplementary material.

Acknowledgements

We thank W. Baehr, P. Detwiler, T. Doan, S. Bajjalieh and A. Polans for comments on the manuscript. We thank Y. Kim, M. Batten, A. Alekseev and M. Kalnoky for technical assistance. Anti-mGluR6 and anti-SV2 antibodies were gifts from S. Nakanishi and S.M. Bajjalieh, respectively. This research was supported by National Institutes of Health grants EY09339 to K.P., EY014561 to F.H., EY11850 to F.R. and NS044922 to A.L., the Whitehall Foundation to A.L., a grant from Research to Prevent Blindness (RPB), Inc. to the Department of Ophthalmology at the University of Washington and a grant from the E.K. Bishop Foundation. K.P. is a RPB Senior Investigator. D.P. was supported by a Vision Core Grant EY01730.

References

1. Zhang N, Townes-Anderson E. Regulation of structural plasticity by different channel types in rod and cone photoreceptors. J Neurosci 2002;22:7065–7079. [PubMed: 12177203]

2. Nachman-Clewner M, St Jules R, Townes-Anderson E. L-type calcium channels in the photoreceptor ribbon synapse: localization and role in plasticity. J Comp Neurol 1999;415:1–16. [PubMed: 10540354]
3. Schmitz F, Konigstorfer A, Sudhof TC. RIBEYE, a component of synaptic ribbons: a protein's journey through evolution provides insight into synaptic ribbon function. Neuron 2000;28:857–872. [PubMed: 11163272]
4. Schmitz Y, Witkovsky P. Dependence of photoreceptor glutamate release on a dihydropyridine-sensitive calcium channel. Neuroscience 1997;78:1209–1216. [PubMed: 9174087]
5. Barnes S, Kelly MEM. Calcium channels at the photoreceptor synapse. in. Photorecept Calcium 2002;514:465–476.
6. Morgans CW. Localization of the α_{1F} calcium channel subunit in the rat retina. Invest Ophthalmol Vis Sci 2001;42:2414–2418. [PubMed: 11527958]
7. McRory JE, et al. The *CACNA1F* gene encodes an L-type calcium channel with unique biophysical properties and tissue distribution. J Neurosci 2004;24:1707–1718. [PubMed: 14973233]
8. Baumann L, Gerstner A, Zong X, Biel M, Wahl-Schott C. Functional characterization of the L-type Ca^{2+} channel $Ca_V1.4\alpha1$ from mouse retina. Invest Ophthalmol Vis Sci 2004;45:708–713. [PubMed: 14744918]
9. Koschak A, et al. $Ca_V1.4\alpha1$ subunits can form slowly inactivating dihydropyridine-sensitive L-type Ca^{2+} channels lacking Ca^{2+}-dependent inactivation. J Neurosci 2003;23:6041–6049. [PubMed: 12853422]
10. Rieke F, Schwartz EA. A cGMP-gated current can control exocytosis at cone synapses. Neuron 1994;13:863–873. [PubMed: 7946333]
11. Bech-Hansen NT, et al. Mutations in *NYX*, encoding the leucine-rich proteoglycan nyctalopin, cause X-linked complete congenital stationary night blindness. Nat Genet 2000;26:319–323. [PubMed: 11062471]
12. Strom TM, et al. An L-type calcium-channel gene mutated in incomplete X-linked congenital stationary night blindness. Nat Genet 1998;19:260–263. [PubMed: 9662399]
13. Ball SL, et al. Role of the β_2 subunit of voltage-dependent calcium channels in the retinal outer plexiform layer. Invest Ophthalmol Vis Sci 2002;43:1595–1603. [PubMed: 11980879]
14. Haeseleer F, et al. Five members of a novel Ca^{2+}-binding protein (CABP) subfamily with similarity to calmodulin. J Biol Chem 2000;275:1247–1260. [PubMed: 10625670]
15. Lee A, et al. Differential modulation of $Ca_V2.1$ channels by calmodulin and Ca^{2+}-binding protein 1. Nat Neurosci 2002;5:210–217. [PubMed: 11865310]
16. Yang J, et al. Identification of a family of calcium sensors as protein ligands of inositol trisphosphate receptor Ca^{2+} release channels. Proc Natl Acad Sci USA 2002;99:7711–7716. [PubMed: 12032348]
17. Haynes LP, Tepikin AV, Burgoyne RD. Calcium-binding protein 1 is an inhibitor of agonist-evoked, inositol 1,4,5-trisphosphate-mediated calcium signaling. J Biol Chem 2004;279:547–555. [PubMed: 14570872]
18. Koulen P, Fletcher EL, Craven SE, Bredt DS, Wassle H. Immunocytochemical localization of the postsynaptic density protein PSD-95 in the mammalian retina. J Neurosci 1998;18:10136–10149. [PubMed: 9822767]
19. Van Hooser JP, et al. Rapid restoration of visual pigment and function with oral retinoid in a mouse model of childhood blindness. Proc Natl Acad Sci USA 2000;97:8623–8628. [PubMed: 10869443]
20. Grunert U, Haverkamp S, Fletcher EL, Wassle H. Synaptic distribution of ionotropic glutamate receptors in the inner plexiform layer of the primate retina. J Comp Neurol 2002;447:138–151. [PubMed: 11977117]
21. Nomura A, et al. Developmentally regulated postsynaptic localization of a metabotropic glutamate receptor in rat rod bipolar cells. Cell 1994;77:361–369. [PubMed: 8181056]
22. Dick O, et al. The presynaptic active zone protein bassoon is essential for photoreceptor ribbon synapse formation in the retina. Neuron 2003;37:775–786. [PubMed: 12628168]
23. Baylor DA, Lamb TD, Yau KW. Responses of retinal rods to single photons. J Physiol (Lond) 1979;288:613–634. [PubMed: 112243]

24. Nakatani K, Yau KW. Calcium and magnesium fluxes across the plasma membrane of the toad rod outer segment. J Physiol (Lond) 1988;395:695–729. [PubMed: 2457685]
25. Field GD, Rieke F. Nonlinear signal transfer from mouse rods to bipolar cells and implications for visual sensitivity. Neuron 2002;34:773–785. [PubMed: 12062023]
26. Slaughter MM, Miller RF. 2-amino-4-phosphonobutyric acid: a new pharmacological tool for retina research. Science 1981;211:182–185. [PubMed: 6255566]
27. Sampath AP, Rieke F. Selective transmission of single photon responses by saturation at the rod-to-rod bipolar synapse. Neuron 2004;41:431–443. [PubMed: 14766181]
28. Pitt GS, et al. Molecular basis of calmodulin tethering and Ca^{2+}-dependent inactivation of L-type Ca^{2+} channels. J Biol Chem 2001;276:30794–30802. [PubMed: 11408490]
29. Erickson MG, Alseikhan BA, Peterson BZ, Yue DT. Preassociation of calmodulin with voltage-gated Ca^{2+} channels revealed by FRET in single living cells. Neuron 2001;31:973–985. [PubMed: 11580897]
30. Zuhlke RD, Pitt GS, Deisseroth K, Tsien RW, Reuter H. Calmodulin supports both inactivation and facilitation of L-type calcium channels. Nature 1999;399:159–162. [PubMed: 10335846]
31. Zhou H, et al. Ca^{2+}-binding protein-1 facilitates and forms a postsynaptic complex with Cav1.2 (L-type) Ca^{2+} channels. J Neurosci 2004;24:4698–4708. [PubMed: 15140941]
32. Baylor DA, Fuortes MG. Electrical responses of single cones in the retina of the turtle. J Physiol (Lond) 1970;207:77–92. [PubMed: 4100807]
33. Pate P, et al. Determinants for calmodulin binding on voltage-dependent Ca^{2+} channels. J Biol Chem 2000;275:39786–39792. [PubMed: 11005820]
34. Peterson BZ, DeMaria CD, Yue DT. Calmodulin is the Ca^{2+} sensor for Ca^{2+}-dependent inactivation of 1-type calcium channels. Neuron 1999;22:549–558. [PubMed: 10197534]
35. Seidenbecher CI, Reissner C, Kreutz MR. Caldendrins in the inner retina. in. Photorecept Calcium 2002;514:451–463.
36. Dolmetsch R. Excitation-transcription coupling: signaling by ion channels to the nucleus. Sci STKE 2003;2003:PE4 . [PubMed: 12538881]
37. Deisseroth K, Heist EK, Tsien RW. Translocation of calmodulin to the nucleus supports CREB phosphorylation in hippocampal neurons. Nature 1998;392:198–202. [PubMed: 9515967]
38. Bading H, Ginty DD, Greenberg ME. Regulation of gene expression in hippocampal neurons by distinct calcium signaling pathways. Science 1993;260:181–186. [PubMed: 8097060]
39. Mao ZX, Bonni A, Xia F, Nadal-Vicens M, Greenberg ME. Neuronal activity-dependent cell survival mediated by transcription factor MEF2. Science 1999;286:785–790. [PubMed: 10531066]
40. Morgans CW, El Far O, Berntson A, Wassle H, Taylor WR. Calcium extrusion from mammalian photoreceptor terminals. J Neurosci 1998;18:2467–2474. [PubMed: 9502807]
41. Morgans CW. Calcium channel heterogeneity among cone photoreceptors in the tree shrew retina. Eur J Neurosci 1999;11:2989–2993. [PubMed: 10457194]
42. Berntson A, Taylor WR, Morgans CW. Molecular identity, synaptic localization, and physiology oOf calcium channels in retinal bipolar cells. J Neurosci Res 2003;71:146–151. [PubMed: 12478624]
43. Bech-Hansen NT, et al. Loss-of-function mutations in a calcium-channel α_1-subunit gene in Xp11.23 cause incomplete X-linked congenital stationary night blindness. Nat Genet 1998;19:264–267. [PubMed: 9662400]
44. Haeseleer F, Imanishi Y, Saperstein DA, Palczewski K. Gene transfer mediated by recombinant baculovirus into mouse eye. Invest Ophthalmol Vis Sci 2001;42:3294–3300. [PubMed: 11726636]
45. Ellis SB, et al. Sequence and expression of messenger RNAs encoding the α_1-subunit and α_2-subunit of a Dhp-sensitive calcium channel. Science 1988;241:1661–1664. [PubMed: 2458626]
46. Perezreyes E, et al. Cloning and expression of a cardiac brain β-subunit of the L-type calcium channel. J Biol Chem 1992;267:1792–1797. [PubMed: 1370480]
47. Haeseleer F, et al. Molecular characterization of a third member of the guanylyl cyclase–activating protein subfamily. J Biol Chem 1999;274:6526–6535. [PubMed: 10037746]
48. Imanishi Y, et al. Characterization of retinal guanylate cyclase–activating protein 3 (GCAP3) from zebrafish to man. Eur J Neurosci 2002;15:63–78. [PubMed: 11860507]

49. Batten ML, et al. Lecithin-retinol acyltransferase is essential for accumulation of all-*trans*-retinyl esters in the eye and in the liver. J Biol Chem 2004;279:10422–10432. [PubMed: 14684738]

50. Maeda T. *et al*. Evaluation of the role of the retinal G protein–coupled receptor (RGR) in the vertebrate retina *in vivo*. J Neurochem 2003;85:944–956. [PubMed: 12716426]

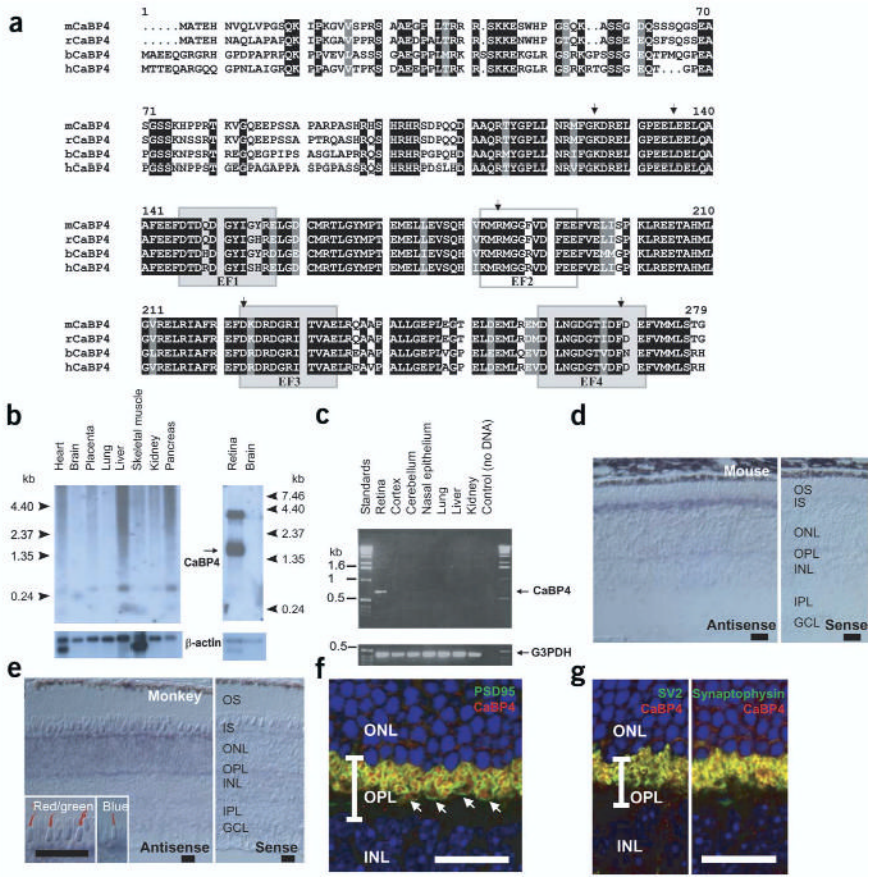

Figure 1.

CaBP4 protein sequence, tissue distribution and immunolocalization. (**a**) Primary structure of mouse (m), rat (r), bovine (b) and human (h) CaBP4 (accession numbers AY039218, XM_344981, AY048883 and AY039271). The identical residues in all sequences are in white on a black background. Conservative substitutions are in white on a gray background. Functional EF-hand motifs are shown as shaded boxes and nonfunctional EF-hand motif as an open box. Arrows indicate the intronexon junction of the *CABP4* gene. (**b**) Northern blot analysis of CaBP4 mRNA from various human (left) or rat (right) tissues. Control hybridization with a ^{32}P-labeled β-actin mRNA is also shown. (**c**) PCR analysis of CaBP4 transcript in various mouse tissues. A positive control was carried out with primers specific for glyceraldehyde-3-phosphate dehydrogenase (G3PDH). (**d**) *In situ* hybridization of CaBP4 transcripts in mouse retina using antisense (left) and sense (right) RNA. (**e**) *In situ* hybridization of CaBP4 transcripts in monkey retina using antisense (left) and sense (right) RNA. Inset, immunoreactivity with antibodies to red and green opsin (left) and blue opsin (right) was covisualized with CaBP4 transcripts (blue signal). (**f**) Presynaptic localization of mouse CaBP4 (red) demonstrated by covisualization with a presynaptic protein (PSD95; green). Arrows indicate rod spherules and cone pedicles. (**g**) Colocalization of synaptic vesicle proteins SV2 and synaptophysin (green) with mouse CaBP4 (red). In **f** and **g**, yellow indicates overlap of two immunoreactivities and blue indicates cell nuclei (Hoechst 33342 staining). INL, inner nuclear layer; ONL, outer nuclear layer; OPL, outer plexiform layer. (**d**–**f**) Scale bars, 20 μm.

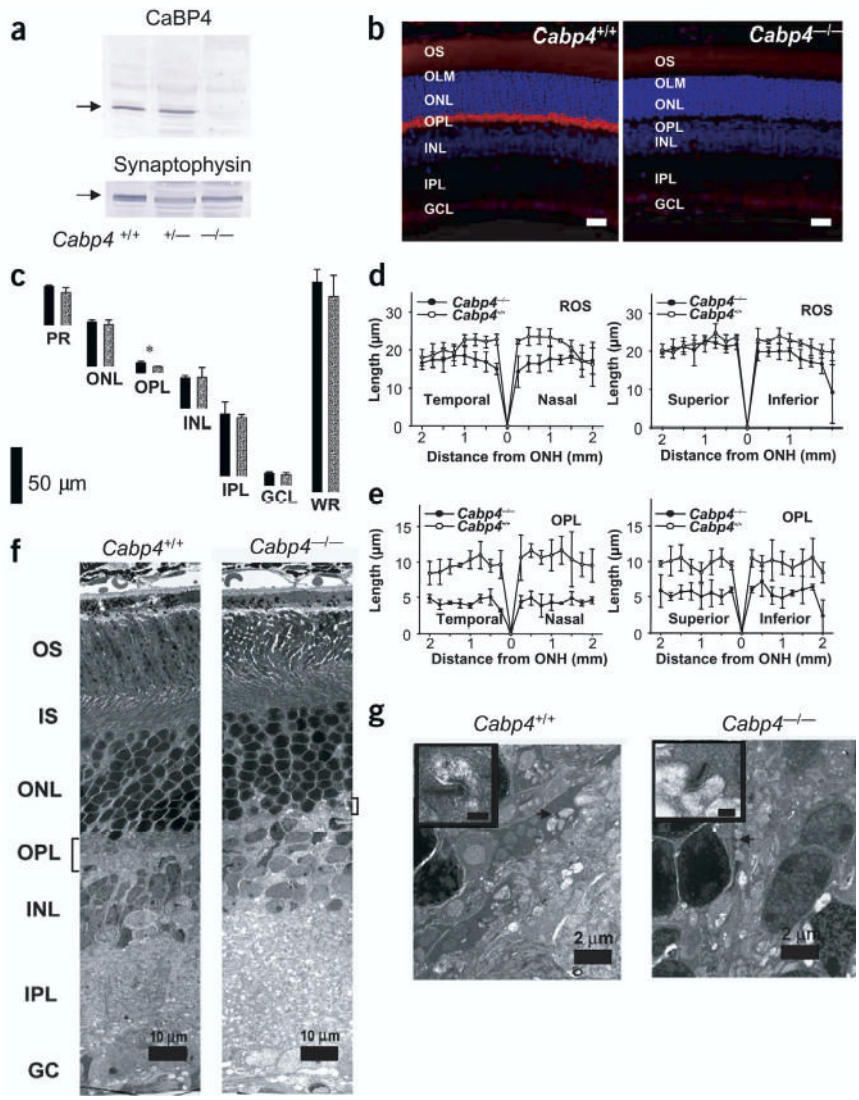

Figure 2.

Characterization of CaBP4 knockout mice. (**a**) Immunoblotting of retinal extracts from *Cabp4*$^{+/+}$, *Cabp4*$^{+/–}$ and *Cabp4*$^{–/–}$ mice probed with anti-CaBP4 or anti-synaptophysin (control). (**b**) Immunolocalization of CaBP4 in the retina of *Cabp4*$^{+/+}$ mouse (left). Lack of CaBP4 immunoreactivity in the retina of *Cabp4*$^{–/–}$ mouse (right). Scale bars, 20 µm. Nuclei are visualized by staining with Hoechst 33342 dye (blue). (**c**) The thickness of individual retinal layers from 8-to 10-week-old *Cabp4*$^{+/+}$ (black bars) and *Cabp4*$^{–/–}$ mice (gray bars) measured at 1.25 mm inferior from the optic nerve head. *$P < 0.01$. GCL, ganglion cell layer; INL, inner nuclear layer; IPL, inner plexiform layer; ONL, outer nuclear layer; OPL, outer plexiform layer; PR, photoreceptor outer and inner segments; WR, whole retina. (**d,e**) Rod outer segment (ROS; **d**) and outer plexiform layer (ORPL; **e**) thickness (in micrometers) plotted as a function of the retinal location (in millimeters) from the optic nerve head. (**f**) Montage of cross-sections through the retinas of 2-month-old mice analyzed by transmission electron microscopy. The outer plexiform layer is thinner in *Cabp4*$^{–/–}$ mice than it is in *Cabp4*$^{+/+}$ mice. IS, inner segment; OS, outer segment. (**g**) Higher magnification of a cross-section through the outer plexiform layer. Photoreceptor terminals are present in the outer plexiform layer of *Cabp4*$^{+/+}$ mice

(arrow), but fewer and altered terminals are observed in *Cabp4*$^{-/-}$ mice. A synaptic ribbon is shown at higher magnification (inset; scale bars, 0.2 μm).

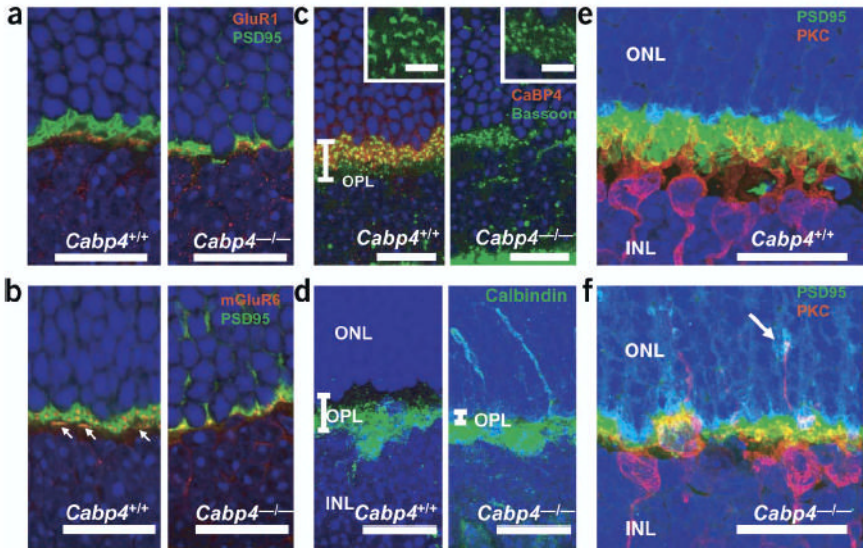

Figure 3.

Synaptic connection between photoreceptors and bipolar cells. (**a**) Immunolocalization of GluR1 (red) and PSD95 (green). In *Cabp4*$^{+/+}$ (left) and *Cabp4*$^{-/-}$ (right) mice, GluR1 is expressed in off-cone bipolar cell dendrites[20] proximal to cone pedicles. PSD95 is localized proximal to the plasma membrane of the photoreceptor synaptic terminals. (**b**) Immunolocalization of mGluR6 (red) and PSD95 (green). A photoreceptor presynapse in a *Cabp4*$^{+/+}$ mouse shows morphologically distinguishable rod spherules and cone pedicles (arrows indicate cone pedicles). *Cabp4*$^{-/-}$ mice have disorganized synaptic processes.(**c**) Immunolocalization of CaBP4 (red) and the presynaptic marker bassoon (green). Insets show higher-magnification images. (**d**) Immunolocalization of calbindin, a marker for H1 horizontal cells. Each picture is a three-dimensional projection made from multiple stacks of confocal images. (**e,f**) Three-dimensional projections of PKCα (red, a marker for rod bipolar cells) and PSD95 (green) immunolocalization in (**e**) *Cabp4*$^{+/+}$ and (**f**) *Cabp4*$^{-/-}$ mice. Arrow indicates ectopic synapse in the outer nuclear layer between rod photoreceptor and bipolar cells. In **a**–**f**, nuclei were visualized by staining with Hoechst 33342 dye. Scale bars, 20 μm (in inset, 5 μm).

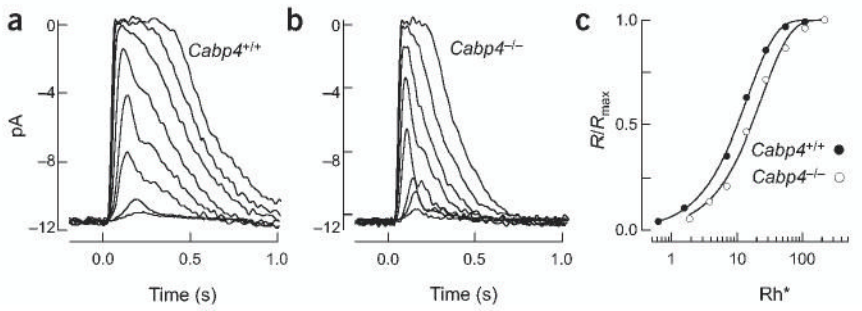

Figure 4.

Current responses of *Cabp4*$^{+/+}$ and *Cabp4*$^{-/-}$ rod outer segments. (**a**) Flash family measured from a *Cabp4*$^{+/+}$ rod. Average responses (5–100 trials at each flash strength) are superimposed for flashes producing 0.65, 1.3, 7, 14, 28, 56, 112 and 224 Rh*. (**b**) Flash family measured from a *Cabp4*$^{-/-}$ rod as in **a**. Flash strengths are 1.9, 3.8, 7.6, 14, 26, 56, 112 and 224 Rh*. (**c**) Stimulus-response relationship for the *Cabp4*$^{+/+}$ (•) and *Cabp4*$^{-/-}$ (○) rod in **a** and **b**. Response amplitudes were normalized to the maximal response and were plotted against flash strength. Saturating exponential fits to the data were used to estimate the half-saturating flash strength.

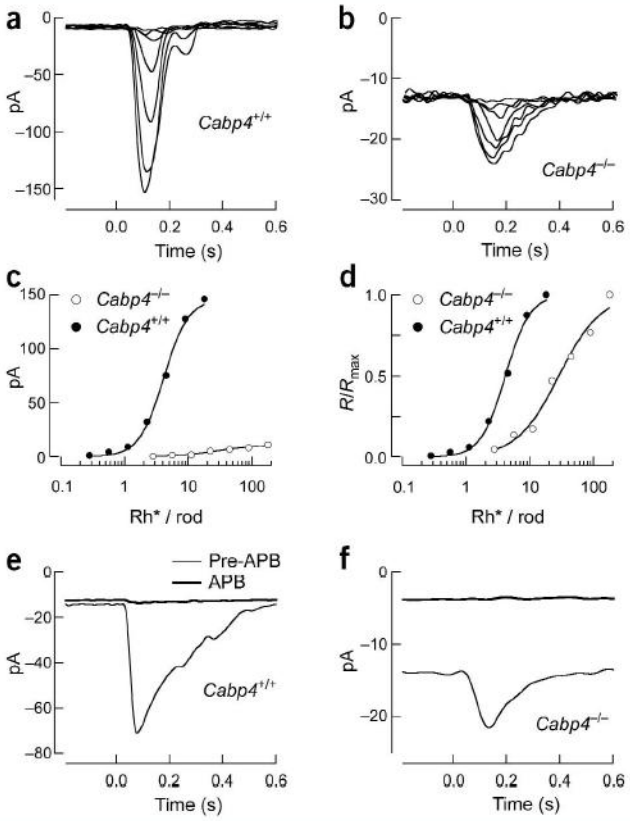

Figure 5.

Voltage-clamp responses of *Cabp4*$^{+/+}$ and *Cabp4*$^{-/-}$ rod bipolars. (**a**) Flash family measured from a *Cabp4*$^{+/+}$ rod bipolar held at −60 mV. Average responses are superimposed for flashes producing 0.28, 0.55, 1.1, 2.2, 4.5, 9 and 18 Rh*/rod. (**b**) Flash family measured from a *Cabp4*$^{-/-}$ rod bipolar as in **a**. Flash strengths are 2.8, 5.6, 11, 22, 44, 90 and 180 Rh*/rod. (**c**) Stimulus-response relationship for the *Cabp4*$^{+/+}$ (•) and *Cabp4*$^{-/-}$ (○) rod bipolar cells in **a** and **b**. (**d**) Stimulus-response relationship as in **c** with the response amplitudes normalized to the maximal response. Hill curves that were fit to the data were used to estimate the half-saturating flash strength. (**e**) Effect of APB on the dark current and saturating response of a *Cabp4*$^{+/+}$ rod bipolar. Saturating flashes producing 36 Rh*/rod were delivered every 3 s. The two traces shown are responses measured before and after adding 8 μM APB to the superfusion solution. (**f**) Effect of APB on the dark current and saturating response of a *Cabp4*$^{-/-}$ rod bipolar, as in **e**. Flash strength was 180 Rh*/rod.

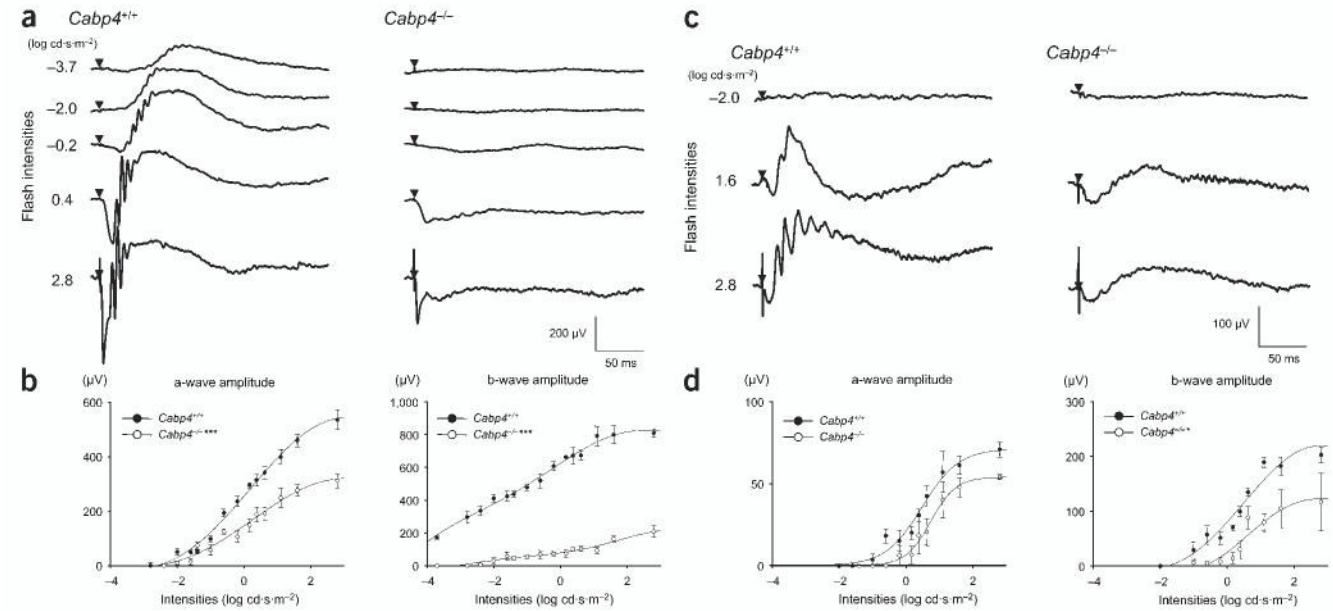

Figure 6.

Single-flash ERG responses of increasing intensity for *Cabp4*$^{-/-}$ and C*abp4*$^{+/+}$ mice. (**a,c**) Serial ERG responses to increasing flash stimuli obtained from *Cabp4*$^{-/-}$ and *Cabp4*$^{+/+}$ mice under (**a**) dark-adapted and (**c**) light-adapted conditions. Single-flash timing is indicated by the filled triangle. (**b**) Plotted ERG a-wave and b-wave amplitudes in response to increasing stimuli in *Cabp4*$^{-/-}$ mice showed significantly lower responses as compared with those in *Cabp4*$^{+/+}$ mice in dark-adapted conditions (***$P < 0.0001$; $n = 8$). (**d**) The b-wave amplitudes in *Cabp4*$^{-/-}$ mice were also lower as compared with those in *Cabp4*$^{+/+}$ mice in light-adapted conditions (*$P < 0.01$; $n = 8$) but the a-wave amplitudes showed smaller differences. Light-adapted responses were examined after bleaching at 1.4 log cd·m^{-2} for 15 min.

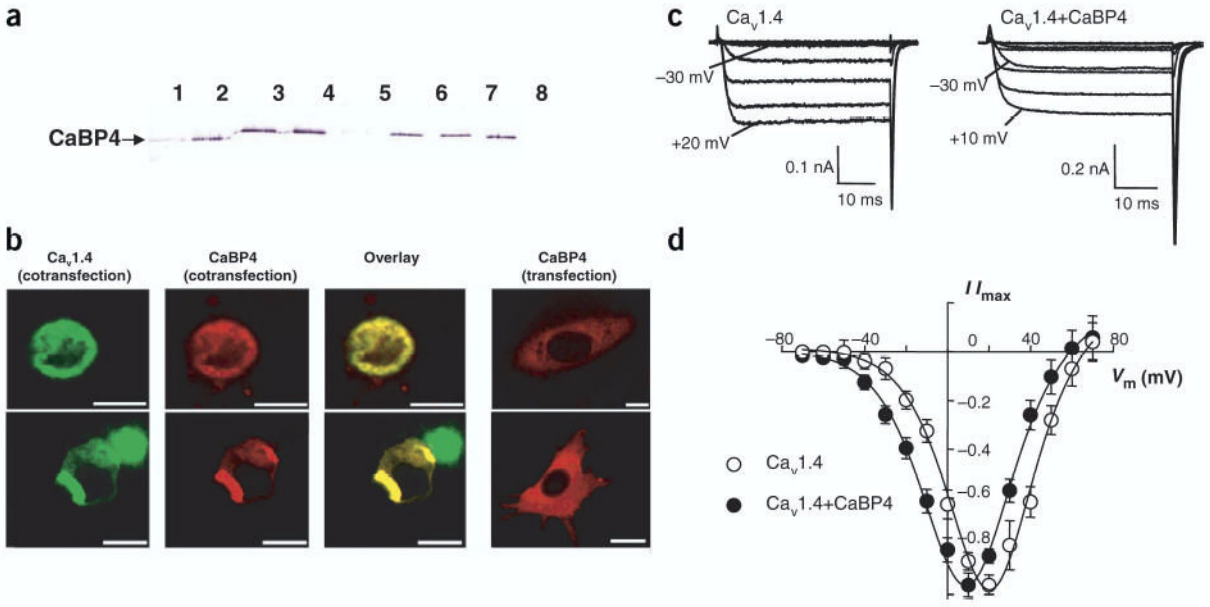

Figure 7.

CaBP4 interacts with and modulates $Ca_v1.4$. (**a**) Affinity chromatography of purified recombinant mCaBP4 on $Ca1.4_v\alpha1$ column. The eluted fractions were probed with anti-CaBP4. Lanes 1–4, elution with 3 mM EGTA; lane 5, final elution with 3 mM EGTA; lanes 6–8: further elution with 0.1 M glycine buffer, pH 2.1. (**b**) Colocalization of CaBP4-DsRed2 with $Ca_v1.4$-GFP in HEK293 cells. Confocal images of HEK293 cells transfected with mCaBP4-DsRed2 and $Ca_v1.4$–GFP (left three panels) or transfected with mCaBP4-DsRed2 alone (right panel). The yellow color indicates colocalization of the overexpressed fusion proteins. Scale bars, 12.5 μ) m. (**c**) Modulation of $Ca_v1.4$ activation by CaBP4 in transfected HEK293T cells. Whole-cell Ca^{2+} currents recorded in cells transfected with $Ca_v1.4$ subunits (α_1 1.4, β_{2A}, $\alpha_2\delta$) alone (left) or cotransfected with CaBP4 (right). Shown are representative traces of Ca^{2+} currents evoked by 50-ms steps from a holding voltage of −80 mV to various test voltages. Extracellular recording solution contained 20 mM Ca^{2+} and intracellular solution contained 5 mM EGTA. CaBP4 enhanced activation of Ca^{2+} currents at negative voltages as indicated. (**d**) Current-voltage relationship from cells transfected with $Ca_v1.4$ alone (○) or cotransfected with CaBP4 (•). For each test voltage (V_m), I/Imax represents the current amplitude measured at 45 ms normalized to the maximal current amplitude obtained in the series (mean ± s.e.m.; n = 7–10).